Inorganic Chemistry

Article

pubs.acs.org/IC

A Porous Metal–Organic Framework Constructed from Carboxylate–Pyrazolate Shared Heptanuclear Zinc Clusters: Synthesis, Gas Adsorption, and Guest-Dependent Luminescent Properties

Qingshu Zheng, Feilong Yang, Mingli Deng, Yun Ling,* Xiaofeng Liu, Zhenxia Chen, Yunhua Wang, Linhong Weng, and Yaming Zhou*

Shanghai Key Laboratory of Molecular Catalysis and Innovative Materials, Department of Chemistry, Fudan University, 220 Handan Road, Shanghai 200433, People's Republic of China

Supporting Information

ABSTRACT: A three-dimensional porous structure of $[Zn_7O_2(bpdc)_4(dmpp)_2]\cdot 6DEF\cdot 10H_2O$ (MAC-7, H_2bpdc = 4,4′-biphenyldicarboxylic acid, Hdmpp = 3,5-dimethyl-4-(4′-pyridyl)pyrazole), built of 12-bridged carboxylate-pyrazolate shared Zn_7O_2 clusters, has been synthesized. Because of the presence of 12-bridged carboxylate-pyrazolate shared building block, MAC-7 is a double-linked *pcu*-type framework and shows reversible phase transformation. Photoluminescent property studies indicate that MAC-7 could sense nitrobenzene over toluene, *p*-xylene, and mesitylene by luminescent quenching.

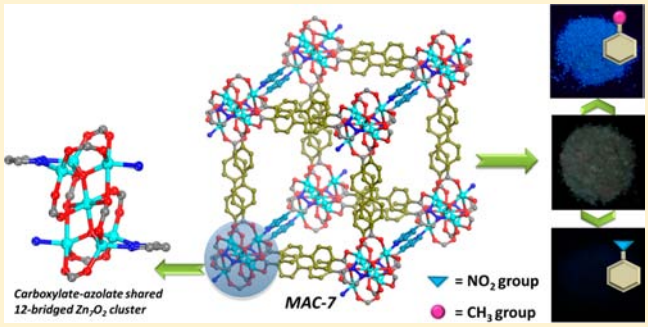

INTRODUCTION

Metal–organic frameworks (MOFs, or porous coordination polymers, PCPs) are usually described as extended networks made of metal clusters as nodes and organic ligands as linkers, in which both metal clusters and organic ligands can be easily exploited.[1] Because of these special advantages, MOFs are fascinating porous materials with designable porous structures[2] and adjustable functions for specific applications.[3]

Metal clusters with well-defined coordination geometries are generally regarded to be one of crucial components in building MOFs, as well as simultaneously introducing essential physical properties such as magnetism,[3h,4] photoluminescence,[3b,5] and unique framework flexibility[6] to these porous structures. The well-defined carboxylate-based metal clusters have been predominantly employed, such as paddle-wheel $[M_2(O_2C)_4]$ units,[7] trigonal $[M_3(\mu_3\text{-}O)(O_2C)_6]$ clusters,[8] and tetragonal $[M_4(\mu_4\text{-}O)(O_2C)_6]$ clusters[9] (where M and O_2C represents the metal center and carboxylate group, respectively). On the other hand, azolate-based ligands such as pyrazolate, triazolate, and tetrazolate are also widely adopted to generate porous structures together with metal ions,[10] and numerous azolate-based metal clusters whose geometries are similar to that of carboxylate-based ones are observed (see Scheme 1). These two types of metal clusters (carboxylate-based and azolate-based) have one common point, and that is the sole kind of coordinated organic groups for a certain metal cluster. To construct novel metal clusters with various coordination groups as well as synthesize multifunctional porous MOFs, considerable efforts have been paid to use mixed carboxylate and azolate ligands or ligands containing multifunctional coordination groups.[11] However, porous structures built of metal clusters containing both carboxyl groups and azole groups are rarely isolated. The carboxylate-azolate shared pinwheel,[12] trinuclear Co_3O,[13] Zn_4O,[14] and Zn_5O_2[15] metal clusters are the limited examples known so far (see Scheme 1).

Scheme 1. General View of Carboxylate-Based, Azolate-Based and Carboxylate-Azolate Shared Metal Clusters Whose Geometries Are Similar to Each Other Based on the Same Number of Metal Centers Reported So Far. (Source: Cambridge Crystallographic Database, February 2013.)

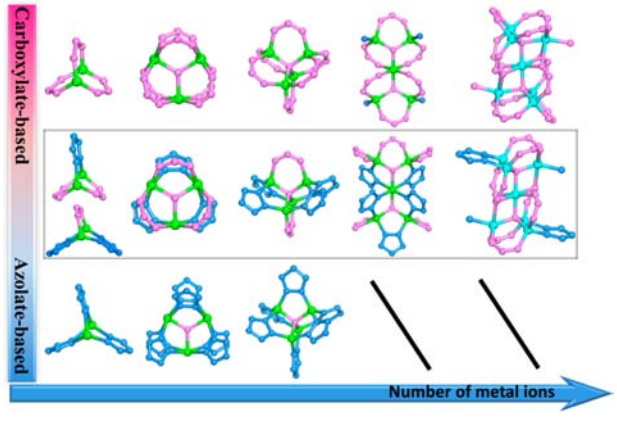

Received: May 2, 2013
Published: September 5, 2013

Our intent is (i) to study the molecular-assembly of ternary components of carboxylate and azolate ligands with metal ions, and (ii) to pursue their porous structures as well as potential applications.[10b,12,16] In this paper, using 4,4′-biphenyldicarboxylic acid (H_2bpdc) and 3,5-dimethyl-4-(4′-pyridyl)pyrazole (Hdmpp) as mixed ligands, a three-dimensional porous structure formulated as $[Zn_7O_2(bpdc)_4(dmpp)_2]\cdot 6DEF\cdot 10H_2O$ (MAC-7, where MAC denotes the metal−azolate−carboxylate framework) has been solvothermally synthesized. It is a *pcu*-type network built of novel carboxylate-pyrazolate shared 12-bridged $[Zn_7(\mu_4\text{-}O)_2(O_2C)_8(NN)_2]$ (Zn_7O_2) metal clusters. Gas adsorption studies confirm its porosity. Furthermore, this porous structure shows interesting guest-dependent photoluminescent properties, which can detect nitrobenzene over toluene, *p*-xylene, and mesitylene by luminescent quenching.

EXPERIMENTAL SECTION

Materials and General Methods. All chemicals were of reagent-grade quality, obtained from commercial sources, and used without further purification. The 3,5-dimethyl-4-(4′-pyridyl)pyrazole ligand was synthesized in the laboratory. Elemental analysis for C, H, N were performed on Elementar Vario EL III system. Fourier transform infrared (FT-IR) spectra were recorded on a Nicolet Avatar-360 FT-IR spectrometer with KBr pellets in the range of 4000−400 cm^{-1}. Powder X-ray diffraction (PXRD) measurements were carried out on a Bruker D8 Advance diffractometer at 40 kV and 40 mA with Cu Kα radiation (λ = 1.5406 Å). Thermogravimetric analysis (TGA) was performed on Model TGA/SDTA 851 thermoanalyzer in the temperature range of 30−800 °C under N_2 flow with a heating rate of 10 °C min^{-1}. Gas adsorption of N_2 at 77 K and a mixture of CO_2, O_2, and N_2 at room temperature were measured on a Micromeretics Model ASAP 2020 gas adsorption analyzer. About 120 mg of supercritical-CO_2 activated samples[17] were degassed at room temperature for 10 h by using the "outgas" function of the surface area analyzer. Helium gas was used to estimate the dead volume. The saturation pressure (P_0) was measured throughout the N_2 analyses via a dedicated saturation pressure transducer, which helps us to monitor the vapor pressure for each data point. Part of the N_2 sorption isotherm in the normalized pressure (P/P_0) range of 0.05−0.3 was used to calculate the BET surface area, and the Langmuir surface area calculation was performed in the low-pressure range. The pore size distribution (PSD) was obtained from the HK model in the Micromeritics ASAP 2020 software package.

The solid samples for photoluminescent measurements were obtained by soaking the activated samples (via supercritical-CO_2 methods) in toluene, *p*-xylene, mesitylene, nitrobenzene, cyclohexane, and tetrahydrofuran (THF) for 1 h, respectively, and then followed by filtration and washed with acetone (3 × 10 mL) to remove the compounds that adsorbed on the surface. The sample was then dried under vacuum at room temperature, to remove acetone. The inclusion of guest molecules was confirmed by thermogravimetric analysis−mass spectrometry (TG-MS) on a coupled system consisting of Model SDT Q600 and GSD 301 T2 under a N_2 atmosphere. Photoluminescence measurements were performed on a Hitachi Model F-4500 fluorescence spectrophotometer equipped with monochromator (resolution = 0.2 nm) and a 150-W Xe lamp at room temperature in solid states. For each testing, ∼45 mg of sample was filled in the solid sample cell. The excitation wavelength was set to be 323 nm, EX slit: 5.0 nm, EM slit: 5.0 nm, PMT voltage: 400 V. Photoluminescent emission is recorded from 350 nm to 600 nm, with a scan speed of 240 nm/min.

Synthesis of 3,5-Dimethyl-4-(4′-pyridyl)pyrazole (Hdmpp).[18] 4-Methylpyridine (11.16 g, 120 mmol) was added to a mixture of acetyl chloride (6.28 g, 80 mmol) and $CHCl_3$ (50 mL) at −20 °C under N_2 atmosphere, and then the mixture was stirred for another 4 h. Pure yellow product of 3-phenylpentane-2,4-dione was obtained by chromatography (V_{hexane}:$V_{ethyl\ acetate}$ = 5:4). The collected 3-phenylpentane-2,4-dione (1.77 g, 10 mmol) was dissolved in toluene solution (20 mL) and then hydrazine hydrate (85%, 0.56 g, 9.5 mmol) was added at room temperature, then the mixture was stirred overnight. Raw products were obtained after evaporation of the solvent. White platelike crystals were obtained by recrystallizing in water. ^{1}H NMR ($CDCl_3$): δ 8.63 (d, 2H, α-Py*H*), 7.24 (d, 2H, β-Py*H*), 2.37 (s, 6H, CH_3).

Preparation of $[Zn_7O_2(bpdc)_4(dmpp)_2]\cdot 6DEF\cdot 10H_2O$ (MAC-7). A mixture of $Zn(NO_3)_2\cdot 6H_2O$ (0.208 g, 0.7 mmol), H_2bpdc (0.097 g, 0.4 mmol), Hdmpp (0.034 g, 0.2 mmol) and *N*,*N*′-diethylformamide (DEF) (10 mL) was stirred at room temperature for 10 min, and then 0.05 mL of HNO_3 was added. The mixture was sealed into a 15-mL Teflon-lined stainless autoclave and heated at 140 °C for 72 h. After cooling to room temperature at a rate of 10 °C h^{-1}, light-yellow block crystals of MAC-7 were collected by filtration and washed with acetone. Yield: 56% based on $Zn(NO_3)_2\cdot 6H_2O$. Elemental analysis for $C_{106}H_{138}N_{12}O_{34}Zn_7$, Calcd. (%): C, 49.32; H, 5.35; N, 6.51; Found: C, 49.41; H, 5.39; N, 6.59. IR (cm^{-1}, KBr): 3430 (b), 2976 (m), 2936 (w), 1659 (s), 1605 (s), 1541 (s), 1401 (s), 1264 (m), 1216 (m), 843 (m), 773 (s), 684 (m), 453 (m).

Single-Crystal X-ray Crystallographic Study. Single-crystal X-ray diffraction of MAC-7 was performed at 173 K on a Bruker Apex Duo diffractometer with graphite-monochromated Mo Kα radiation (λ = 0.71073 Å). Data collection and reduction were performed using the APEX II software. Multiscan absorption corrections were applied for all the datasets using the APEX II program. The structures were solved by direct methods and refined by least-squares on F^2 using the SHELXTL program package.[19] All non-hydrogen atoms were refined with anisotropic displacement parameters. Hydrogen atoms attached to carbon were placed in geometrically idealized positions and refined using a riding model. PLATON/SQUEEZE program[20] was used to remove the disordered solvent molecules in the channels. The numbers of guest molecules were calculated according to thermogravimetric analysis and EA results. Crystallographic data are listed in Table 1, and selected bond length and angles are listed in Table S1 in the Supporting Information.

RESULTS AND DISCUSSION

Synthesis. It has been well-known that amides such as *N*,*N*′-dimethylformamide (DMF) and *N*,*N*′-diethylformamide (DEF) can provide an efficient solvent environment for the assembly of high nucleated metal clusters as well as isolation of their pure crystal phases. Detectable crystals of MAC-7 could be isolated when DMF was used as the solvent. However, the PXRD patterns revealed the impurity of as-made products. To obtain the phase-pure bulk samples, adjusting the mole ratio of the reactants or changing the reaction temperature in the case of DMF solvent were tried, but failed. Phase-pure bulk samples

Table 1. Crystallographic Data for MAC-7 after PLATON/SQUEEZE

parameter	value/comment
compound	MAC-7
empirical formula	$C_{76}H_{52}N_6O_{18}Zn_7$
formula weight	1794.97 g mol^{-1}
temperature	173(2) K
wavelength	0.71073 Å
crystal system	triclinic
space group	$P\bar{1}$(2)
a	12.880(3) Å
b	16.861(3) Å
c	17.325(3) Å
α	75.74(3)°
β	73.26(3)°
γ	68.59(3)°
V	3311.9(14) Å^3
Z	1
ρ (g cm^{-3})	0.900
μ (mm^{-1})	1.287
GOF on F^2	1.030
$R_1{}^a$ [$I > 2\sigma(I)$]	0.0765
$wR_2{}^b$ (all data)	0.2363

$^aR_1 = \sum||F_o| - |F_c||/\sum|F_o|$. $^bwR_2 = [\sum w(F_o^2 - F_c^2)^2/\sum w(F_o^2)^2]^{1/2}$.

were obtained by using DEF as solvent and followed by 0.05 mL HNO_3 when the molar ratio of reactants was set to be 4:2:7 (H_2bpdc:Hdmpp:$Zn(NO_3)_2{\cdot}6H_2O$).

Structural Characterization. Single-crystal X-ray diffraction (SC-XRD) study reveals that MAC-7 crystallizes in triclinic system, $P\bar{1}$ space group (see Table 1), and is a three-dimensional porous structure based on 12-bridged carboxylate-pyrazolate shared $[Zn_7(\mu_4\text{-}O)_2(O_2C)_8(NN)_2]$ clusters (Zn_7O_2, Figure 1). This novel cluster is composed of two asymmetric $[Zn_4(\mu_4\text{-}O)(O_2C)_4(NN)]$ motifs by sharing a six-coordinated Zn(4) metal ion at an inversion center (see Figure S1 in the Supporting Information). The μ_4-O(1) connects to the four Zn(II) ions with an average Zn−O(1) bond distance of ca. 1.93 Å (see Table S1 in the Supporting Information for details), which is close to that of Zn_4O cluster in MOF-5 (ca. 1.94 Å).[9a] Zn(1) and Zn(2) adopt four-coordinated tetrahedral geometries, and Zn(3) is in five-coordinated tetragonal pyramid geometry (see Figure S1 in the Supporting Information). All the Zn−N and Zn−O bond distances are in the normal range, except the Zn(3)−O(2) bond (2.552 Å), which is slightly longer than the others. These four Zn(II) ions are further bridged in pairs by one pyrazolate group from the dmpp linker and four carboxylate groups from the bpdc linkers, generating the asymmetric $[Zn_4(\mu_4\text{-}O)(O_2C)_4(NN)]$ motif. After a symmetric operation via the inversion center at Zn(4) site, the carboxylate-pyrazolate shared 12-bridged $[Zn_7(\mu_4\text{-}O)_2(O_2C)_8(NN)_2]$ cluster is formed. Based on the two types of coordinated organic groups of carboxylates and pyrazolates, four dmpp and eight bpdc ligands then periodically connect the Zn_7O_2 cluster in six directions, generating the double-linked *pcu*-type framework with 3D intersection channels (see Figure 1b). The windows sizes are measured to be approximately 7.6 Å × 8.4 Å, 4.6 Å × 5.0 Å, and 3.0 Å × 6.2 Å along the *a*-, *b*-, and *c*-axis, respectively (taking the van der Waals radii into account).

High nuclear metal clusters with well-defined geometries are very important for the design and synthesis of porous structures. The metal clusters constructed by various

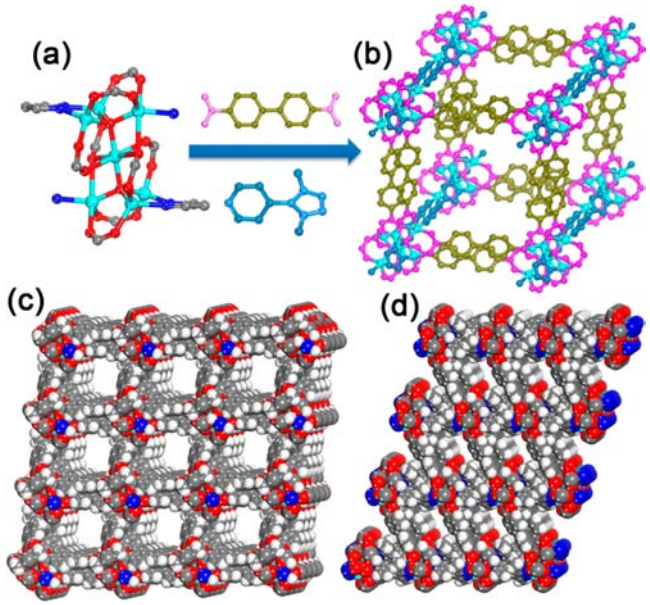

Figure 1. (a) The 12-bridged $[Zn_7(\mu_4\text{-}O)_2(O_2C)_8(NN)_2]$ metal cluster based on two $[Zn_4(\mu_4\text{-}O)(O_2C)_4(NN)]$ clusters with a shared Zn(4) site on the inversion center. (b) The double-walled *pcu*-type framework of MAC-7 based on Zn_7O_2 cluster connected by pbdc and dmpp ligands. (c) The space-filling model of the three-dimensional (3D) porous structure of MAC-7 along the *a*-axis. (d) The space-filling model of the 3D porous structure of MAC-7 along the *c*-axis.

coordination groups might be of great interest for the design of multivariate functions in a certain prototype framework. Qiu and Zhu first reported the carboxylate-based Zn_7O_2 cluster in the structure of $[Zn_7O_2(pda)_5(H_2O)_2]$[21] (see Figure 2a). Kim and Shimizu then observed the reversible interpenetration in $[Zn_7O_2(NBD)_5(DMF)_2]$.[22] The reported carboxylate-based

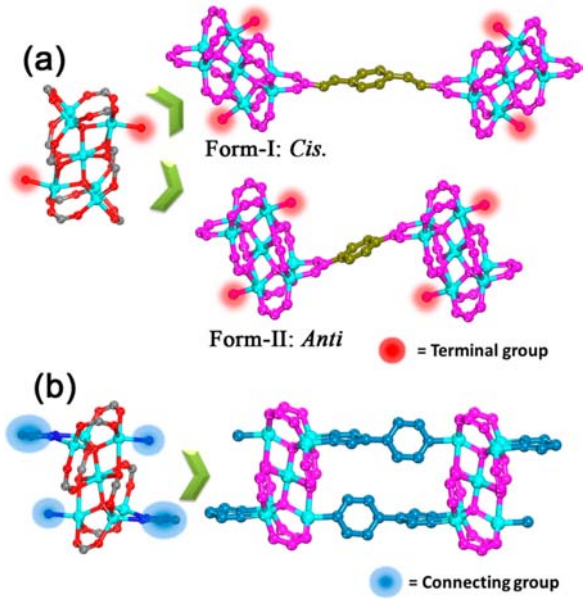

Figure 2. (a) The 10-connected carboxylate-based Zn_7O_2 cluster, which only can be linked by single carboxylate linker in one direction with either *cis* or *anti*-configuration, because of the presence of a terminal group. (b) The 12-bridged carboxylate-azolate shared Zn_7O_2 cluster, which can be linked symmetrically by double dmpp ligands, because of its precisely designed coordination geometry.

dx.doi.org/10.1021/ic401092j | Inorg. Chem. 2013, 52, 10368−10374

Zn_7O_2 cluster can be viewed as the fusion of two Zn_4O clusters at a shared Zn(II) site. Because of the presence of coordinated terminal group of H_2O or DMF, the carboxylate-based Zn_7O_2 cluster shows a 10-connected node (see Figure 2a). While in MAC-7, two pairs of carboxylates and a terminal coordinated group in the 10-connected carboxylate-based Zn_7O_2 cluster are replaced by the pyrazolate and pyridine motifs of dmpp ligands. As a result, the carboxylate-pyrazolate shared Zn_7O_2 cluster transforms to be a 12-bridged node with two types of coordinated organic ligands (Figure 2b). The high connected metal clusters and the presence of coordinated azolate groups may enhance the framework stability, compared with that of the only carboxylate-based one.[12−15]

Thermogravimetric Analysis (TGA) and Powder X-ray Diffraction (PXRD). TGA (Figure 3a) shows that there is a weight loss of 30.5% from room temperature to 200 °C for the as-made MAC-7, which can be ascribed to the release of guest molecules (calculated 30.4%), then remains stable up to 420 °C. After that, a huge weight loss is observed, suggesting the decomposition of the entire framework. After the removal of guest molecules, the high decomposition temperature is further confirmed by its TGA curve. Compared to the decomposition temperature of carboxylate-based Zn_7O_2 framework (~380 °C),[21] MAC-7 shows higher thermal stability.

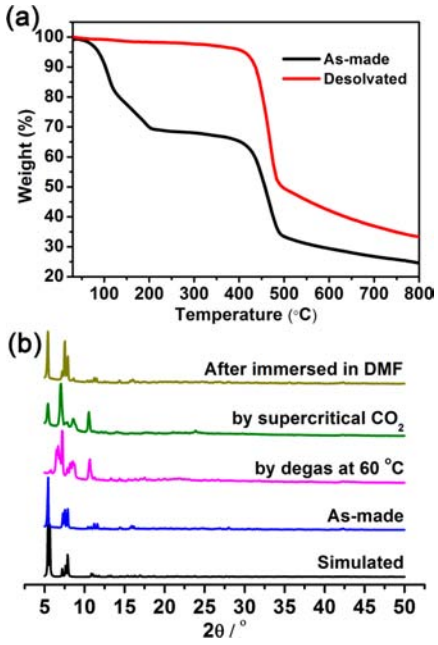

Figure 3. (a) TGA curves of as-made and desolvated MAC-7. (b) PXRD patterns of as-made MAC-7, which is consistent with that of the simulated one, and observable phase transformation was observed after degassing at 60 °C, compared to that treated by supercritical CO_2, and the framework can return to its original phase by soaking in DMF solvent.

The PXRD pattern of as-made sample matches well with the simulated one based on the CIF, showing the strong diffraction peak at $2\theta \approx 5.4°$ (Figure 3b), except losing the diffraction signal at $2\theta \approx 5.6°$. The peaks at $2\theta \approx 5.4°$ and 5.6° are the diffraction planes of [001] and [010] (see Figure S2 in the Supporting Information), which corresponds to the periodic arrangements of large channels (7.6 Å × 8.4 Å) along the *c*- and *b*-axes, respectively. The loss of the diffraction peak at $2\theta \approx 5.6°$ suggests the possible adjustment of the large channel, which could be ascribed to the dynamic structural transformation of MAC-7 at room temperature, compared with the crystal structure detected at 173 K. The structural transformation can be further confirmed by the PXRD pattern of thermally treated MAC-7. After MAC-7 was degassed at 60 °C overnight, the PXRD pattern shifts greatly and the peak at $2\theta \approx 5.4°$ disappears, indicating the occurrence of the structural transformation. These results indicate that MAC-7 is a flexible framework, to some extent. Remarkably, it can recover to its original crystal phase after being immersed into toluene or DMF for 1 h, which was confirmed by the PXRD pattern (Figure 3b). Compared with the porous structures based on the carboxylate-based Zn_7O_2 clusters, the reversible framework transformation could be ascribed to the presence of coordinated azolate groups in the metal cluster, which enhance the framework stability.[3c,11] In addition, the sample activated using the supercritical CO_2 method continues to have a better structural orientation, compared to the sample activated by degassing at 60 °C, although a broadening and slight shifts of the peaks are also observed (see Figure 3b).

Gas Adsorption. To assess the porosity of MAC-7, N_2 adsorption at 77 K was performed on samples activated by supercritical CO_2 (Figure 4a). The Brunauer−Emmett−Teller (BET) surface area is 533 m^2/g (803 m^2/g, using the Langmuir methodology). The average pore size (as determined using the Horvath−Kawazoe method) is ~6.8 Å, and the pore volume (using the t-Plot method) is ~0.13 $cm^3\ g^{-1}$. The surface area is much smaller than the theoretically calculated accessible surface area of 1744 $m^2\ g^{-1}$ (see Figure S3 in the Supporting Information).[23] We ascribe the low BET surface area to the structural transformation after removal of guest molecules, while partial collapse of the host frameworks could not be excluded. In addition, the step adsorption in the P/P_0 range of 0.1−0.4 and large hysteresis of desorption isotherm also confirm the framework flexibility, to some extent.[22b,24]

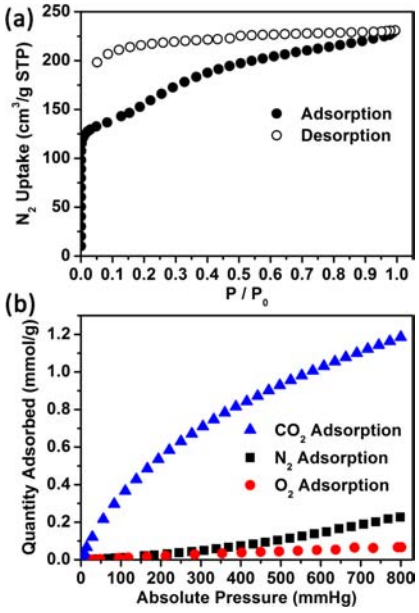

Figure 4. (a) N_2 sorption curve of activated MAC-7 at 77 K; (b) CO_2, N_2, and O_2adsorption of activated MAC-7 at 298 K. MAC-7 was activated by supercritical CO_2.

The sorption of CO_2, O_2, and N_2 at room temperature was then carried out on the activated sample. The results (Figure

dx.doi.org/10.1021/ic401092j | Inorg. Chem. 2013, 52, 10368−10374

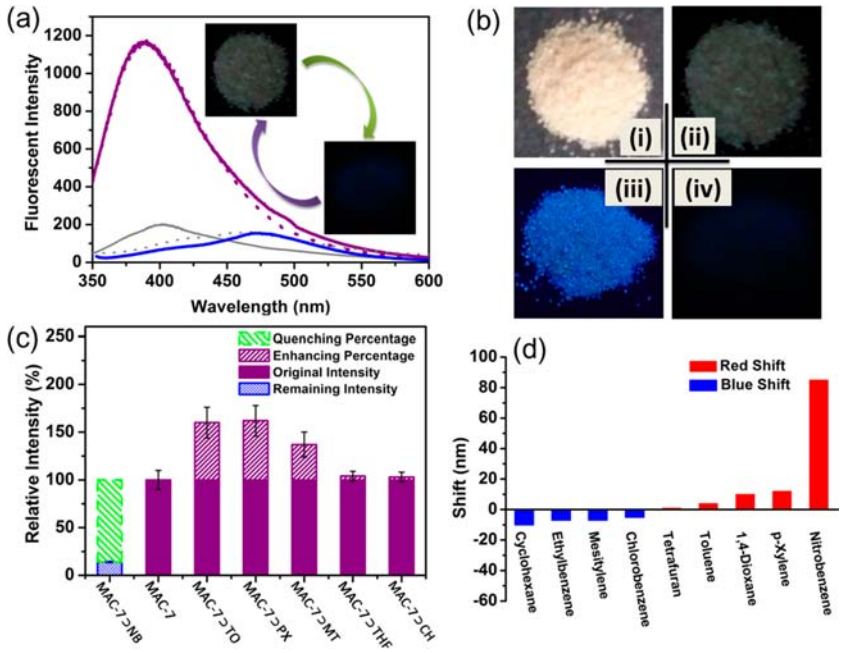

Figure 5. (a) Photoluminescent emission of MAC-7 (solid purple curve), after inclusion of NB showing photoluminescent quenching (solid gray curve), red-shift with times (solid blue curve) and photoluminescent emission recovers by immersed into DMF (dot purple curve). (b) Optical photographs of (i) the as-made sample under sun light, (ii) the as-made sample under UV irradition, (iii) MAC-7⊃TO under UV irradiation, and (iv) MAC-7⊃NB under UV irradiation. (c) Comparison of photoluminescent emissions of MAC-7⊃NB with that of MAC-7⊃TO, MAC-7⊃PX, MAC-7⊃TM, MAC-7⊃THF, MAC-7⊃CH, and MAC-7. (d) Red-shift of MAC-7 after the inclusion of NB (85 nm), compared with other molecules.

4b) indicate that the framework of MAC-7 shows nil adsorption of N_2 and O_2 at room temperature, and the uptake amount is ca. 0.23 and 0.07 mmol/g at a pressure of 800 mmHg, respectively. On the other hand, the uptake amount of CO_2 increases quickly as the pressure increases, and it reaches to ca. 1.19 mmol/g at 800 mmHg. In the case of post-combustion CO_2 capture, the partial pressures of CO_2, N_2, and O_2 are ∼0.15, 0.75, and 0.03 bar, respectively.[3a] The selectivity of CO_2 over N_2 and O_2, based on the single-component adsorption results, was simply calculated using

$$S = \frac{x_1/y_1}{x_2/y_2}$$

where S is the selectivity factor, x_i represents the quantity adsorbed of component i, and y_i represents the partial pressure of component i. The selectivity of CO_2 over N_2 is ∼17, and the selectivity of CO_2 over O_2 is ∼57; this suggests the potential selective adsorption[3f,2S] of CO_2 over N_2 and O_2.

Guest-Dependent Luminescent Properties. Upon excitation at λ_{ex} = 323 nm, solid sample of MAC-7 shows a fluorescent emission with the maximum peak at λ_{em} = 390 nm (Figure 5a). To understand its emission mechanism, the photoluminescent emission of ligands in their solid states and in solution (DMAC, $c = 1.0 \times 10^{-5}$ mol/L) were studied respectively (Figure S4). In solid states, emission peaks at 410 and 408 nm are observed for H_2bpdc and Hdmpp, respectively, which are very close to that of MAC-7. In the DMAC solution, the emission of H_2bpdc is similar to that in the solid state with a peak at 407 nm. However, Hdmpp gives the maximum emission peak at 475 nm, which shows a large red shift, compared to that in the solid state. Based on these studies, we ascribe the emission of MAC-7 to the intraligand fluorescent emission of ligands in their close packing states. To explore the possible guest-dependent luminescent behaviors, three types of guest molecules were chosen: (i) aromatics with electron-withdrawing groups, (ii) aromatics with electron-donating groups, and (iii) aromatics with nonconjugated compounds. The activated MAC-7 was immersed in nitrobenzene (NB), toluene (TO), *p*-xylene (PX), mesitylene (MT), cyclohexane (CH), and tetrahydrofuran (THF), for 1 h each. The related samples were labeled as MAC-7⊃NB, MAC-7⊃TO, MAC-7⊃PX, MAC-7⊃MT, MAC-7⊃CH and MAC-7⊃THF, respectively. Their framework integrities were confirmed by PXRD patterns (see Figure S5 in the Supporting Information). The inclusion of these guest molecules was confirmed by TG-MS measurements (see Figure S6 in the Supporting Information).

Considering the possible deviation of fluorescent intensity between different batch samples of MAC-7, solid-state photoluminescent measurements were carried out in three parallels before and after the inclusion of guests (NB, TO, PX, MT, CH, THF). In each group, the photoluminescent intensity of desolvated MAC-7 was set to be 100%, and then the photoluminescent intensity after the inclusion of guests was compared to that value. Upon excitation at λ_{ex} = 323 nm, the fluorescent emission of MAC-7 ⊃ TO, MAC-7 ⊃ PX, and MAC-7 ⊃ MT is observed at λ_{em} = 400, 393, and 401 nm, respectively, which is close to that of MAC-7 (see Figure S7 in the Supporting Information). The intensity of the fluorescent emission is enhanced accordingly: 60% ± 16% for MAC-7 ⊃ TO, 62% ± 16% for MAC-7 ⊃ PX, and 37% ± 13% for MAC-7 ⊃ MT (see Figure 5c). However, for MAC-7 ⊃ NB, ∼90% ± 2% quenching and an ∼13-nm red-shift are observed, compared with that of MAC-7. In addition, the different optic phenomena could also be identified by their optic pictures under UV conditions (see Figure 5b). Here, CH and THF were used as reference probe molecules, because of their nonconjugated

dx.doi.org/10.1021/ic401092j | *Inorg. Chem.* 2013, 52, 10368−10374

structures (see Figure S7 in the Supporting Information). There are no obvious changes in intensity for MAC-7 ⊃ CH and MAC-7 ⊃ THF. Therefore, the observable changes in fluorescent intensity for MAC-7 ⊃ TO, MAC-7 ⊃ PX, MAC-7 ⊃ MT, and MAC-7 ⊃ NB could be ascribed to the presence of a $\pi-\pi$ stacking interaction between the incorporated aromatics and the host framework, which makes the ligand-to-ligand charge transform (LLCT) possible. The enhancement in the case of toluene, xylene, and mesitylene, and the quenching in the case of nitrobenzene, could be related to the donor–acceptor electron-transfer mechanism.[5b] The obvious quenching phenomenon for nitrobenzene suggests that MAC-7 could be used as a potential luminescent sensor for detecting nitrobenzene molecules. It is interesting to note that the red shift of the emission peak of MAC-7 ⊃ NB gradually moves to lower energy regions when we prolonged the soaking time, and the shift reaches 85 nm after 10 h (see Figure 5d). However, for other small organic molecules, such obvious red-shifts were not observed (see Figure 5d, as well as Figure S8 in the Supporting Information). Furthermore, the luminescent emission of MAC-7 ⊃ NB could recover to its original position after being reimmersed in DMF solution for 10 h (see Figure 5a), suggesting that MAC-7 can be reversibly used for the sensing of NB.

CONCLUSION

In this paper, using 4,4′-biphenyldicarboxylic acid (H_2bpdc) and 3,5-dimethyl-4-(4′-pyridyl)pyrazole (Hdmpp) as mixed ligands, a three-dimensional porous structure of $[Zn_7O_2(bpdc)_4(dmpp)_2]\cdot 6DEF\cdot 10H_2O$ (MAC-7) has been synthesized, which is built of novel 12-bridged carboxylate–pyrazolate shared Zn_7O_2 metal clusters. Gas adsorption results confirmed its porosity. Because of the unique Zn_7O_2 cluster, the framework exhibits high thermal stability and reversible phase transformation. Guest-dependent luminescent property of MAC-7 indicates that MAC-7 can serve as a promising candidate for sensing nitrobenzene via fluorescent quenching, compared with other aromatics. Further extensive research work on tuning the two types of extendable ligands for the specific applications are undertaken in our group.

ASSOCIATED CONTENT

Supporting Information

A CIF file, tables, and figures are provided as Supporting Information. This material is available free of charge via the Internet at http://pubs.acs.org.

AUTHOR INFORMATION

Corresponding Author

*E-mail addresses: yunling@fudan.edu.cn (Y.L.), ymzhou@fudan.edu.cn (Y.Z.).

Notes

The authors declare no competing financial interests.

ACKNOWLEDGMENTS

We gratefully acknowledge the financial support from NSFC (Nos. 21201039, 21101031, and 21203032), the Shanghai Leading Academic Discipline Project (No. B108), and the Program for Changjiang Scholars and Innovative Research Team in University (No. IRT1117).

REFERENCES

(1) (a) Paz, F. A.; Klinowski, J.; Vilela, S. M.; Tome, J. P.; Cavaleiro, J. A.; Rocha, J. *Chem. Soc. Rev.* **2012**, *41*, 1088–1110. (b) Tranchemontagne, D. J.; Mendoza-Cortes, J. L.; O'Keeffe, M.; Yaghi, O. M. *Chem. Soc. Rev.* **2009**, *38*, 1257–1283. (c) Kitagawa, S.; Kitaura, R.; Noro, S. *Angew. Chem., Int. Ed.* **2004**, *43*, 2334–2375.

(2) (a) O'Keeffe, M.; Yaghi, O. M. *Chem. Rev.* **2012**, *112*, 675–702. (b) Perry, Iv, J. J.; Feng, P. L.; Meek, S. T.; Leong, K.; Doty, F. P.; Allendorf, M. D. *J. Mater. Chem.* **2012**, *22*, 10235–10248.

(3) (a) Sumida, K.; Rogow, D. L.; Mason, J. A.; McDonald, T. M.; Bloch, E. D.; Herm, Z. R.; Bae, T.-H.; Long, J. R. *Chem. Rev.* **2012**, *112*, 724–781. (b) Cui, Y. J.; Yue, Y. F.; Qian, G. D.; Chen, B. L. *Chem. Rev.* **2012**, *112*, 1126–1162. (c) Wu, H.; Gong, Q.; Olson, D. H.; Li, J. *Chem. Rev.* **2012**, *112*, 836–868. (d) Kreno, L. E.; Leong, K.; Farha, O. K.; Allendorf, M.; Van Duyne, R. P.; Hupp, J. T. *Chem. Rev.* **2012**, *112*, 1105–1125. (e) Horcajada, P.; Gref, R.; Baati, T.; Allan, P. K.; Maurin, G.; Couvreur, P.; Ferey, G.; Morris, R. E.; Serre, C. *Chem. Rev.* **2012**, *112*, 1232–1268. (f) Li, J. R.; Kuppler, R. J.; Zhou, H. C. *Chem. Soc. Rev.* **2009**, *38*, 1477–1504. (g) Murray, L. J.; Dinca, M.; Long, J. R. *Chem. Soc. Rev.* **2009**, *38*, 1294–1314. (h) Kurmoo, M. *Chem. Soc. Rev.* **2009**, *38*, 1353–1379.

(4) (a) Coronado, E.; Espallargas, G. M. *Chem. Soc. Rev.* **2013**, *42*, 1525–1539. (b) Wang, Z. M.; Hu, K. L.; Gao, S.; Kobayashi, H. *Adv. Mater.* **2010**, *22*, 1526–1533. (c) Zeng, M. H.; Wang, B.; Wang, X. Y.; Zhang, W. X.; Chen, X. M.; Gao, S. *Inorg. Chem.* **2006**, *45*, 7069–7076.

(5) (a) Cui, J.; Lu, Z.; Li, Y.; Guo, Z.; Zheng, H. *Chem. Commun.* **2012**, *48*, 7967–7969. (b) Pramanik, S.; Zheng, C.; Zhang, X.; Emge, T. J.; Li, J. *J. Am. Chem. Soc.* **2011**, *133*, 4153–4155. (c) Xu, H.; Liu, F.; Cui, Y.; Chen, B.; Qian, G. *Chem. Commun.* **2011**, *47*, 3153–3155. (d) Jiang, H.-L.; Tatsu, Y.; Lu, Z.-H.; Xu, Q. *J. Am. Chem. Soc.* **2010**, 5586–5587. (e) Lan, A.; Li, K.; Wu, H.; Olson, D. H.; Emge, T. J.; Ki, W.; Hong, M.; Li, J. *Angew. Chem., Int. Ed.* **2009**, *48*, 2334–2338.

(6) (a) Fletcher, A. J.; Thomas, K. M.; Rosseinsky, M. J. *J. Solid State Chem.* **2005**, *178*, 2491–2510. (b) Uemura, K.; Matsuda, R.; Kitagawa, S. *J. Solid State Chem.* **2005**, *178*, 2420–2429.

(7) (a) Chen, B. L.; Xiang, S. C.; Qian, G. D. *Acc. Chem. Res.* **2010**, *43*, 1115–1124. (b) Eddaoudi, M.; Kim, J.; Wachter, J. B.; Chae, H. K.; O'Keeffe, M.; Yaghi, O. M. *J. Am. Chem. Soc.* **2001**, *123*, 4368–4369.

(8) (a) Bury, W.; Chwojnowska, E.; Justyniak, I.; Lewinski, J.; Affek, A.; Zygadlo-Monikowska, E.; Bak, J.; Florjanczyk, Z. *Inorg. Chem.* **2012**, *51*, 737–745. (b) Serre, C.; Mellot-Draznieks, C.; Surble, S.; Audebrand, N.; Filinchuk, Y.; Ferey, G. *Science* **2007**, *315*, 1828–1831.

(9) (a) Li, H.; Eddaoudi, M.; O'Keeffe, M.; Yaghi, O. M. *Nature* **1999**, *402*, 276–279. (b) Spanopoulos, I.; Xydias, P.; Malliakas, C. D.; Trikalitis, P. N. *Inorg. Chem.* **2013**, *52*, 855–862. (c) Brozek, C. K.; Dincă, M. *Chem. Sci.* **2012**, *3*, 2110–2113.

(10) (a) Zhang, J. P.; Zhang, Y. B.; Lin, J. B.; Chen, X. M. *Chem. Rev.* **2012**, *112*, 1001–1033. (b) Ling, Y.; Zhai, F.-P.; Deng, M.-L.; Wu, D.; Chen, Z.-X.; Liu, X.-F.; Zhou, Y.-M.; Weng, L.-H. *CrystEngComm* **2012**, *14*, 1425–1431. (c) Ling, Y.; Chen, Z.-X.; Zhou, Y.-M.; Weng, L.-H.; Zhao, D.-Y. *CrystEngComm* **2011**, *13*, 1504–1508. (d) Jeong, S.; Song, X.; Oh, M.; Liu, X.; Kim, D.; Moon, D.; Lah, M. S. *Inorg. Chem.* **2011**, *50*, 12133–12140. (e) Dinca, M.; Yu, A. F.; Long, J. R. *J. Am. Chem. Soc.* **2006**, *128*, 8904–8913.

(11) (a) Yang, E.; Li, H.-Y.; Wang, F.; Yang, H.; Zhang, J. *CrystEngComm* **2013**, *15*, 658–661. (b) Senchyk, G. A.; Lysenko, A. B.; Krautscheid, H.; Rusanov, E. B.; Chernega, A. N.; Kramer, K. W.; Liu, S. X.; Decurtins, S.; Domasevitch, K. V. *Inorg. Chem.* **2013**, *52*, 863–872. (c) Cui, G.-H.; He, C.-H.; Jiao, C.-H.; Geng, J.-C.; Blatov, V. A. *CrystEngComm* **2012**, *14*, 4210–4216. (d) Zhong, D.-C.; Deng, J.-H.; Luo, X.-Z.; Liu, H.-J.; Zhong, J.-L.; Wang, K.-J.; Lu, T.-B. *Cryst. Growth Des.* **2012**, *12*, 1992–1998. (e) Procopio, Q. E.; Fukushima, T.; Barea, E.; Navarro, J. A.; Horike, S.; Kitagawa, S. *Chem.—Eur. J.* **2012**, *18*, 13117–13125. (f) Montoro, C.; Linares, F.; Procopio, E. Q.; Senkovska, I.; Kaskel, S.; Galli, S.; Masciocchi, N.; Barea, E.; Navarro, J. A. *J. Am. Chem. Soc.* **2011**, *133*, 11888–11891. (g) Eubank, J. F.; Wojtas, L.; Hight, M. R.; Bousquet, T.; Kravtsov, V.; Eddaoudi, M. *J. Am. Chem. Soc.* **2011**, *133*, 17532–17535. (h) Procopio, Q. E.; Linares,

F.; Montoro, C.; Colombo, V.; Maspero, A.; Barea, E.; Navarro, J. A. *Angew. Chem., Int. Ed.* **2010**, *49*, 7308−7311.
(12) Ling, Y.; Chen, Z.; Zheng, H.; Zhou, Y.; Weng, L.; Zhao, D. *Cryst. Growth Des.* **2011**, *11*, 2811−2816.
(13) Aharen, T.; Habib, F.; Korobkov, I.; Burchell, T. J.; Guillet-Nicolas, R.; Kleiz, F.; Murugesu, M. *Dalton Trans.* **2013**, *42*, 7795−7802.
(14) Hou, L.; Lin, Y. Y.; Chen, X. M. *Inorg. Chem.* **2008**, *47*, 1346−1351.
(15) Gao, W. Y.; Yan, W.; Cai, R.; Meng, L.; Salas, A.; Wang, X. S.; Wojtas, L.; Shi, X.; Ma, S. *Inorg. Chem.* **2012**, *51*, 4423−4425.
(16) (a) Xia, B.; Chen, Z.; Zheng, Q.; Zheng, H.; Deng, M.; Ling, Y.; Weng, L.; Zhou, Y. *CrystEngComm* **2013**, *15*, 3484−3489. (b) Ling, Y.; Yang, F.; Deng, M.; Chen, Z.; Liu, X.; Weng, L.; Zhou, Y. *Dalton Trans.* **2012**, *41*, 4007−4011. (c) Ling, Y.; Chen, Z.-X.; Zhai, F.-P.; Zhou, Y.-M.; Weng, L.-H.; Zhao, D.-Y. *Chem. Commun.* **2011**, *47*, 7197−7199. (d) Ling, Y.; Zhang, L.; Li, J.; Du, M. *CrystEngComm* **2011**, *13*, 768−770.
(17) Nelson, A. P.; Farha, O. K.; Mulfort, K. L.; Hupp, J. T. *J. Am. Chem. Soc.* **2009**, *131*, 458−460.
(18) (a) Hou, L.; Shi, W.-J.; Wang, Y.-Y.; Wang, H.-H.; Cui, L.; Chen, P.-X.; Shi, Q.-Z. *Inorg. Chem.* **2011**, *50*, 261−270. (b) Cui, Q.; Cao, X.-Y.; Tang, L.-F. *Polyhedron* **2005**, *24*, 209−214.
(19) Sheldrick, G. M. *Acta Crystallogr., Sect. A: Found. Crystallogr.* **2008**, *64*, 112−122.
(20) (a) Spek, A. L. *Acta Crystallogr., Sect. D: Biol. Crystallogr.* **2009**, *65*, 148−155. (b) Spek, A. L. *J. Appl. Crystallogr.* **2003**, *36*, 7−13.
(21) Fang, Q. R.; Zhu, G. S.; Xue, M.; Zhang, Q. L.; Sun, J. Y.; Guo, X. D.; Qiu, S. L.; Xu, S. T.; Wang, P.; Wang, D. J.; Wei, Y. *Chem.—Eur. J.* **2006**, *12*, 3754−3758.
(22) (a) Iremonger, S. S.; Vaidhyanathan, R.; Mah, R. K.; Shimizu, G. K. H. *Inorg. Chem.* **2013**, *52*, 4124−4126. (b) Choi, S. B.; Furukawa, H.; Nam, H. J.; Jung, D. Y.; Jhon, Y. H.; Walton, A.; Book, D.; O'Keeffe, M.; Yaghi, O. M.; Kim, J. *Angew. Chem., Int. Ed.* **2012**, *51*, 8791−8795.
(23) Düren, T.; Millange, F.; Férey, G.; Walton, K. S.; Snurr, R. Q. *J. Phys. Chem. C* **2007**, *111*, 15350−15356.
(24) (a) Tanaka, D.; Nakagawa, K.; Higuchi, M.; Horike, S.; Kubota, Y.; Kobayashi, T. C.; Takata, M.; Kitagawa, S. *Angew. Chem., Int. Ed.* **2008**, *47*, 3914−3918. (b) Zhao, X.; Xiao, B.; Fletcher, A. J.; Thomas, K. M.; Bradshaw, D.; Rosseinsky, M. J. *Science* **2004**, *306*, 1012−1015.
(25) (a) An, J.; Geib, S. J.; Rosi, N. L. *J. Am. Chem. Soc.* **2010**, *132*, 38−39. (b) Li, J. R.; Sculley, J.; Zhou, H. C. *Chem. Rev.* **2012**, *112*, 869−932. (c) Xiang, S. C.; He, Y. B.; Zhang, Z. J.; Wu, H.; Zhou, W.; Krishna, R.; Chen, B. L. *Nat. Commun.* **2012**, *3*, 954. (d) Ferey, G.; Serre, C.; Devic, T.; Maurin, G.; Jobic, H.; Llewellyn, P. L.; De Weireld, G.; Vimont, A.; Daturi, M.; Chang, J. S. *Chem. Soc. Rev.* **2011**, *40*, 550−562. (e) Bae, Y. S.; Snurr, R. Q. *Angew. Chem., Int. Ed.* **2011**, *50*, 11586−11596. (f) D'Alessandro, D. M.; Smit, B.; Long, J. R. *Angew. Chem., Int. Ed.* **2010**, *49*, 6058−6082.